

Degradation of ciprofloxacin by persulfate activated by Fe (Ⅱ) doped BiOCl composite photocatalyst

Gen Liu (✉ 18353120186@163.com)

Northeast Normal University

Yingzi Lin

Jilin Jianshu University <https://orcid.org/0000-0003-1792-4982>

Siwen Li

Northeast Normal University

Chunyan Shi

Kitakyushu Shiritsu Daigaku - Hibikino Campus

Dongyan Zhang

Jilin Jianshu University

Lei Chen

Jilin Jianshu University

Research Article

Keywords:

Posted Date: October 29th, 2022

DOI: <https://doi.org/10.21203/rs.3.rs-1789983/v1>

License:   This work is licensed under a Creative Commons Attribution 4.0 International License.

[Read Full License](#)

Version of Record: A version of this preprint was published at Environmental Science and Pollution Research on July 11th, 2023. See the published version at <https://doi.org/10.1007/s11356-023-28490-0>.

Abstract

Fe-BOC-X photocatalyst was successfully prepared by solvothermal method. The photocatalytic activity of Fe-BOC-X was determined by ciprofloxacin (CIP), a typical fluoroquinolone antibiotic. Under sunlight irradiation, all Fe-BOC-X showed better CIP removal performance than original BiOCl. In comparison, the photocatalyst with iron content of 50 wt% (Fe-BOC-3) has excellent structural stability and the best adsorption photodegradation efficiency. The removal rate of CIP (10 mg/l) by Fe-BOC-3 (0.6 g/L) reached 81.4% within 90 min. At the same time, the effects of photocatalyst dosage, pH, persulfate, persulfate concentration and combinations of different systems (PS, Fe-BOC-3, Vis/PS, Vis/Fe-BOC-3, Fe-BOC-3/PS and Vis/Fe-BOC-3/PS) on the reaction were systematically discussed. Reactive species trapping experiments, electron spin resonance (ESR) signals revealed that the photo-generated holes (h^+), hydroxyl radical ($\bullet OH$), sulfate radical ($\bullet SO_4^-$) and superoxide radical ($\bullet O_2^-$) played an important role in CIP degradation, hydroxyl radicals ($\bullet OH$) and sulfate radicals ($\bullet SO_4^-$) play a major role. Various characterization methods have demonstrated that Fe-BOC-X has larger specific surface area and pore volume than original BiOCl. UV-vis DRS indicate that Fe-BOC-X has wider visible light absorption and faster photocarrier transfer, and provides abundant surface oxygen absorption sites for effective molecular oxygen activation. Accordingly, a large number of active species were produced and participated in the photocatalytic process, thus effectively promoting the degradation of ciprofloxacin. Based on HPLC-MS analysis, two possible decomposition pathways of CIP were finally proposed. The main degradation pathways of CIP are mainly due to the high electron density of piperazine ring in CIP molecule, which is mainly attacked by various free radicals. The main reactions include piperazine ring opening, decarbonylation, decarboxylation and fluorine substitution. This study can better open up a new way for the design of visible light driven photocatalyst and provide more ideas for the removal of CIP in water environment.

1. Introduction

With the improvement of social public health and safety awareness and the upgrading of detection and analysis technology, more and more kinds and frequencies of new organic pollutants are detected in the water environment. Emerging pollutants (ECS) refer to a series of newly detected pollutants in the environment. They are usually not under the supervision of the government or environmental protection department. They exist in the environment at a low concentration (usually detected in low concentrations in the range of ng ng/L or $\mu\text{g/L}$), but pose a great health risk to human body and ecosystem (Kumar et al. 2019, Reichert et al. 2019). Emerging pollutants that have been reported include endocrine disruptors (EDCs) (Walpen et al. 2021), pharmaceuticals and personal care products (PPCPs) (Jin et al. 2022, Li et al. 2021, Yao et al. 2022), perfluoroalkyl substances (Wang et al. 2021, Zhao et al. 2021b), brominated flame retardants (BRPs) (Feiteiro et al. 2021), disinfection by-products of drinking water (DBPs), nano materials (NMS), micro plastics (MP) (Llorca et al. 2017, Zhuang et al. 2022). Among them, PPCPs and EDCs are incorporated into persistent organic compounds by the Stockholm Convention signed by the United Nations. PPCPs are widely detected and persist in natural water bodies. They will enter the human

body through water, food and skin care products, and pose a serious threat to the ecological environment and human health because of their bioaccumulation, persistence and biodegradability, Therefore, the removal of PPCPs from water has attracted more and more attention.

Ciprofloxacin (CIP), a third-generation quinolones with broad-spectrum antibacterial activity (Guellati et al. 2022, Yu et al. 2019b), is a frequently used anti biological for human and veterinary illness. Ciprofloxacin has 2–4 times higher antibacterial activity than norfloxacin and enoxacin. In addition, ciprofloxacin is one of the quinolone antibiotics widely used in the pharmaceutical industry because of its high curative effect and low price. It is mainly used to treat urinary tract infection, skin infection and various bacterial infections.

Ciprofloxacin, as an antibiotic, can effectively inhibit and treat bacterial infections (Zhou & Kang 2013) and protect people's health, however, the pollution hazards at this stage should not be underestimated (Riaz et al. 2017, Zhang et al. 2019b). According to studies, ciprofloxacin cannot be completely metabolized in the human body or other organisms, and about 70% of CIP will be discharged into wastewater in the form of active drug and eventually flow into the ecological environment (Githinji et al. 2010). At present, ciprofloxacin has been detected in surface water (Yan et al. 2013, Zhang et al. 2013), various sewage (Herrera-Herrera et al. 2010) and aquaculture areas (Castrignano et al. 2020, Zou et al. 2011) to varying degrees. Long-term existence of ciprofloxacin will produce certain toxic effects on aquatic organisms (Sharma et al. 2016). This shows that the treatment of ciprofloxacin in water is imperative, Therefore, the effective mineralization of antibiotics from wastewater has become utmost necessary for living organism and environment. Scholars have explored a series of technical methods to solve the problems of ciprofloxacin in water.

To date, many methods have been developed to remove CIP from water, including microbial methods (Fan et al. 2019), adsorption (Yu et al. 2019a, Zhao et al. 2022), photocatalytic degradation (Liu et al. 2021a, Zhao et al. 2021a), advanced oxidation (Chen et al. 2020, Chen et al. 2022), electrocatalysis (Zhang et al. 2020a) and so on. Photocatalysis is one of the advanced oxidation processes (AOPs) for the removal of different organic pollutants from water, which has attracted much attention because of its easy handling, selectivity, and environmental friendliness. The commonly used photocatalytic materials are TiO₂, CdO, CdS, ZnO, Fe₃O₄, CuO, BiVO₄, BiOCl and so on. among them, BiOCl, which has many advantages such as easy preparation method, low price and stable chemical properties, is greatly favored by researchers. BiOCl is a white crystalline powder that is nontoxic and normally only responds to UV light. BiOCl is a kind of ternary oxide from family $A_2B_2O_7$, and the inner typical layered structure is formed by the interdigitation of Cl⁻ ion layer and [Bi₂O₂]²⁺ layer (Wang et al. 2017), and this special crystal structure produces an inner electrostatic field which facilitates the efficient separation of photogenerated carriers and improves the activity of BiOCl photocatalysts (Sharma et al. 2019, Zhang et al. 2019a).

At present, the preparation methods of BiOCl photocatalysts generally include solvothermal method (Gu et al. 2017, Zhou et al. 2020), room temperature hydrolysis method (Tian et al. 2019, Zhu et al. 2019), precipitation method (Paul Chowdhury & Shambharkar 2019, Zhang et al. 2020b), hydrothermal synthesis

method (Adhikari & Kim 2018, Li et al. 2020), etc. Through different preparation methods, BiOCl photocatalyst will show different morphologies, and its photocatalytic performance will also show different differences. Zhou (Zhou et al. 2020) and other researchers used ethylene glycol as solvent to prepare three-dimensional BiOCl microspheres with an average particle size of 1.73 nm by solvothermal method. Gu (Gu et al. 2017) and other researchers used the general solvothermal method to synthesize the flower like BiOCl photocatalyst composed of pure phase nanosheets. Zhu (Zhu et al. 2019) and other researchers successfully synthesized Cds/BiOCl thin film photocatalyst through two-step hydrothermal and hydrolysis methods. Tian (Tian et al. 2019) and other researchers successfully prepared flower shaped BiOCl by a simple one-step room temperature method. Zhang (Zhang et al. 2020b) and other researchers synthesized BiOCl/CeO₂ composites with high specific surface area and low band gap by a simple one-step coprecipitation method. Arpita (Paul Chowdhury & Shambharkar 2019) and other researchers successfully prepared a new BiOCl/CoWO₄ heterostructure photocatalyst by chemical precipitation method. Li (Li et al. 2020) and other researchers synthesized a new C-BiOCl photocatalyst with glucose as carbon source by hydrothermal method. Adhikari (Adhikari & Kim 2018) and other researchers prepared BiOCl/WO₃ composites with larger surface area by using a variety of surfactants through one-step hydrothermal synthesis. For semiconductors with large band gap (such as ZnO, TiO₂), the spectral absorption range is narrow and only responds to strong radiation; For semiconductors with small band gap (such as CdS, BiVO₄, BiOCl, etc.), although they can absorb visible light or even infrared light, it also means that the oxidation-reduction ability is weakened. At the same time, the electron hole structure produced by semiconductor materials is also very easy to composite, and the composite speed is very fast, so it is not conducive to the removal of pollutants. In recent years, researchers have made in-depth research on the preparation method, photocatalytic reaction mechanism and application of BiOCl, but BiOCl still has some problems, such as poor visible light utilization, low photocatalyst activity and inconvenient recycling, which can not meet the requirements of practical application. If you want to improve the catalytic activity of BiOCl photocatalytic materials, you can use the following technical methods: metal doping and deposition, heterostructure construction, non-metal doping, morphology control, etc.

In addition, the emerging persulfate advanced oxidation process is mostly used to treat refractory organic compounds in water, which mainly uses sulfate radical ($\bullet SO_4^-$) as the main active substance in the system. $\bullet SO_4^-$ is produced by activating persulfate (PMS) and persulfate (PS) to participate in the degradation reaction (Fernandes et al. 2018). Compared with PMS, PS has a longer bond length and requires less energy to produce $\bullet SO_4^-$. Because $\bullet SO_4^-$ as higher oxidation capacity and longer half-life than $\bullet OH$ (Ghanbari & Moradi 2017), it greatly enhances the utilization of oxidants and can effectively degrade organic pollutants. Therefore, the advanced oxidation technology using persulfate system has attracted much attention. At present, common methods for activating persulfate include UV activation (Gao et al. 2019, Wang et al. 2020), thermal activation (Ji et al. 2015, Sun et al. 2019b), alkali activation (Dominguez et al. 2020, Huang et al. 2020, Lominchar et al. 2018), transition metal activation (Li et al. 2017, Wang et al. 2018, Weng & Tao 2018), carbon based material activation (Carpio et al. 2018, Guo et al. 2018, Tang et al. 2021), etc.

In this Research, BiOCl photocatalyst was prepared by hydrothermal synthesis. In order to change the catalytic activity of BiOCl, Fe () doped element was used to prepare Fe BiOCl photocatalyst. The prepared photocatalyst materials were characterized by XRD, SEM, TEM, EDS, bet, XPS, UV Vis DRS and other analytical means to explore the structural morphology, specific surface area, visible light absorption capacity and other properties of the photocatalyst. With ciprofloxacin (CIP) as the target pollutant, a reaction system was constructed by using the prepared photocatalyst and persulfate. The photocatalytic experiment of CIP degradation was carried out under the irradiation of xenon lamp simulating visible light, and the effects of different influencing factors on CIP removal rate were explored to determine the optimal degradation system. At the same time, the optimal degradation system was used for free radical capture experiment, EPR analysis and biological acute toxicity detection to explore the reaction mechanism of the composite photocatalysis system and the changes of biological acute toxicity. The intermediate products of CIP degradation in Vis/Fe-BOC-3/PS system were explored and analyzed by mass spectrometry, and the possible degradation path of CIP in this system was inferred.

2. Materials and Methods

2.1 Materials

In this research, deionized water was used as the solvent, ciprofloxacin (analytical pure) McLean Biochemical Technology Co., LTD. Bismuth Nitrate (analytical pure) Sinopharm Chemical Reagent Co., LTD. Ferric nitrate (analytical pure) Sinopharm Chemical Reagent Co., LTD. KCL (analytical pure); Tianjin Guangfu Fine Chemical Research Institute; Tianjin Guangfu Fine Chemical Research Institute; Sodium persulfate (analytically pure) Shanghai Aladdin Reagent Co., LTD. Xilong Scientific Co.,Ltd.; Xilong Scientific Co.,Ltd.; Hydrochloric acid (analytical pure) Beijing Chemical Plant; Naoh (analytically pure) Beijing Chemical Plant; Ammonium oxalate (analytically pure), Tianjin Guangfu Fine Chemical Research Institute; Tert-butanol (analytically pure); Tianjin Institute of Fine Chemicals; P-benzoquinone (analytical pure), Tianjin Guangfu Fine Chemical Research Institute; Formic acid (analytically pure) Beijing Chemical Plant; Methanol (chromatographic pure) Marida Technology Co., LTD. Acetonitrile (chromatographic pure) Mairuida Technology Co., LTD. The light-emitting bacteria freeze-dried powder is Eclox.

2.2 Preparation of photocatalyst

Dissolve 2 mM of bismuth nitrate pentahydrate and different mass of ferric nitrate hexahydrate (8, 16, 24, 32 mg) in 0.1 M mannitol and stir for 60 min, then add 2 mM of potassium chloride and stir for 60 min. after all the reagents are dissolved, put them into a 100 mL reactor, set the temperature at 160 °C, and the reaction time is 12 h. After the reaction is completed, the reactor is cooled to room temperature, the suspension in the reactor is centrifugally washed with deionized water and anhydrous ethanol for three times, and the obtained precipitation product is placed in the oven at 80 °C for 12 h. after drying, it is ground to the white powder without particles and sealed for standby. The composite catalysts are named as Fe-BiOCl-1, Fe-BiOCl-2, Fe-BiOCl-3 and Fe-BiOCl-4 (Fe-BOC-1, Fe-BOC-2, Fe-BOC-3 and Fe-BOC-4 for

short). The difference between the preparation of BiOCl and the above is that ferric nitrate is not added before the reaction.

2.3 Characterization

The X-ray diffraction (XRD) patterns of the samples were obtained using a Bruker D8 Advance X-ray diffractometer with Cu K α radiation with scan angles ranging from 0° to 90°. The morphologies and microstructures of the as-prepared samples were analysed via scanning electron microscopy (SEM, FEI S-4800, America) and transmission electron microscopy (TEM, JEOL JEM-2100). The specific Brunauer Emmett Teller (BET) surface area of the as-prepared samples were measured by nitrogen adsorption-desorption isotherms methods using Micrometrics ASAP 2020. The valence states of the elements were documented by a Thermo Fisher Escalab 250XI X-ray photoelectron spectrometer (XPS) with C 1s to calibrate peak positions. The UV-vis diffuse reflectance spectra (UV-vis DRS) were recorded by a Japanese Hitachi U-4100. The steady-state photoluminescence (PL) spectra were measured by a DR-6000 fluorescence spectrophotometer with excitation wavelength of 350 nm. Electron Paramagnetic Resonance (EPR, Bruker EMX PLUS) was applied to detect reactive oxygen species generated in the photocatalytic system with 5, 5-dimethyl-1-pyrroline-N-oxide (DMPO) as the radicals spin-trapped reagent under visible light. Quantitative EPR measurements were performed by using 50 mg portions of samples.

2.4 Photocatalysis experiments on ciprofloxacin degradation

PL-X300D xenon lamp is used to simulate visible light in this experiment. CIP is used as the target pollutant. 10mg CIP solid powder is dissolved in 1L deionized water to prepare 10mg/L CIP reaction solution. Weigh photocatalysts with different dosage into CIP reaction solution with initial concentration of 10 mg/L. In order to make the catalyst and CIP solution reach the adsorption desorption equilibrium state, conduct dark adsorption reaction for 30 min. A xenon lamp with a power of 300 W was used as the light source to simulate visible light in the experiment. The reaction time was 90 min. in the photocatalysis experiment, the solution samples were taken every 15 min. after 0.22 μ m organic filter membrane filtration, the concentration of CIP was detected by a DR-6000 UV-vis spectrophotometer at characteristic wavelength of 276 nm. The degradation efficiency (η) of CIP was calculated as follows.

$$\eta(\%) = (C_t - C_0) / C_0 \times 100\%$$

1

Where C_0 and C_t were the concentrations of CIP in the reaction aqueous solution, respectively.

In order to explore the cycle ability and stability of photocatalyst, four cycle experiments were set up in this study. The solution sample after 90 min reaction is washed with deionized water for many times, centrifuged, and dried in a blast oven at 80 °C to obtain a photocatalyst sample. Ensure that the experimental conditions are consistent for each cycle experiment.

Langmuir-H kinetic model was used to fit the CIP degradation process of photocatalyst(Miao et al. 2019),and the Pseudo-First-Order kinetic model was used to analyze the influence of different photocatalyst activated persulfate systems on CIP degradation rate. Pseudo-First-Order dynamics fitting formula is as follows:

$$\ln(C_t/C_0) = -kt$$

2

Where k and t were the kinetic constant and the reaction time, respectively.

2.5 Acute toxicity test of Luminescent bacteria

In order to explore the changes of biological acute toxicity before and after the degradation of ciprofloxacin solution, Lumistox300 analyzer was used to evaluate the toxicity of *Vibrio Fischeri* (lyophilized). Specific experimental operation: in the refrigerator at minus 18°C, first take out a bottle of bacterial resuscitation solution and let it stand for 5–10 min to restore it to room temperature; Then, take out a bottle of freeze-dried luminescent bacteria (*Vibrio Fischeri*) from the refrigerator, quickly suck 1mL of cell resuscitation solution restored to room temperature and add it to the freeze-dried bacteria, shake it for 1–3 min to make the bacteria fully fuse with the resuscitation solution to make a bacterial suspension, and wait for the recovery of the bacteria. After 30 minutes of culture, the cell luminescence was recorded. Luminescence inhibition rate was calculated as follows.

$$\text{Inhibition rate} = (C_0 - C_{30}) / C_0 \times 100\%$$

3

Where C_0 and C_{30} were the the luminous intensity of the blank solution (RLU) and the luminous intensity of the sample at 30 min (RLU), respectively.

2.6 Identification of the degradation intermediates

The intermediate products were identified by high performance liquid chromatography-mass spectrometry (HPLC-MS) on Agilent C_{18} column (150 mm × 4.6mm, 3.5 μm), the column temperature is set to 30 °C. The mobile phase was composed of 0.1% formic acid and acetonitrile (20:80), the flow rate was 0.4 mL/min, and the injection volume was 30 μL. The ionization mode is EIS⁺, the mass charge ratio scanning range is 50–500, and the fragmentation voltage is 90V.

2.7 Identification of free radicals

Electron paramagnetic resonance (EPR) infers the main active substances in the reaction system. Electron Paramagnetic Resonance (EPR, Bruker EMX PLUS) was applied to detect reactive oxygen species generated in the photocatalytic system with 5, 5-dimethyl-1-pyrroline-N-oxide (DMPO) as the radicals spin-trapped reagent under visible light. The test conditions are: the central magnetic field is

3500 G; the scanning width is 100 G; the energy is 6.33 mW; the resonance frequency is 9.82 GHz; the scanning time is 30 s.

3. result and discussion

3.1 Photocatalysts characterization

In order to study the composition and phase structure of the catalyst samples, XRD was used to characterize the prepared powder photocatalyst. The catalyst samples characterized are BiOCl, Fe-BOC-1, Fe-BOC-2, Fe-BOC-3 and Fe-BOC-4. The XRD results of characterization are shown in Fig. 2. The crystal structure and main species composition of the photocatalyst can be clearly seen in Fig. 2. It is observed that the prepared catalyst was observed to be located at $2\theta = 11.98^\circ$, 25.86° , 32.49° , 33.44° , 40.89° and 46.63° appeared sharp diffraction peaks. These characteristic diffraction peaks can directly correspond to (001), (101), (110), (102), (112) and (200) crystal planes respectively, conform to the crystal structure of BiOCl, and basically conform to the BiOCl standard card (JCPDS No.06-0249) (Tian et al. 2019, Zhang et al. 2020b). With the gradual increase of iron doping content, the diffraction peaks of Fe-BOC-1, Fe-BOC-2, Fe-BOC-3 and Fe-BOC-4 composite catalysts are also basically consistent with the standard card diffraction peaks of BiOCl, and there is no iron oxide or other impurity peak. It is worth noting that, compared with BiOCl, Fe-BOC-1, Fe-BOC-2, Fe-BOC-3 and Fe-BOC-4 are found at 32.49° , and the characteristic diffraction peaks of the four composite catalyst samples doped with iron elements shift slightly to the left. This phenomenon may be because Fe^{3+} doping in the lattice of BiOCl replaces some Bi atoms in the lattice, changes the cell parameters of the catalyst, and shifts the XRD diffraction peaks (Di et al. 2015). Because iron doping is highly dispersed in the catalyst and the doping content is low, the characteristic peak of iron element hybrid can not be detected, which is consistent with the results of EDS mapping and XPS.

3.2 Morphology analysis of photocatalyst

In order to examine the morphology and micro-structure of the as-prepared materials, SEM and HR-TEM analysis were performed. The catalyst samples characterized were BiOCl and Fe-BOC-3.

Figure 3(a, b) shows that pure BiOCl is mainly formed by the accumulation of a series of circular cake fragments with uniform size distribution. After the introduction of Fe element, the morphology of the catalyst basically did not change greatly, but only showed some slight changes. As can be seen from Fig. 3(c, d), although the overall morphology of Fe-BOC-3 catalyst still showed a pie structure similar to that of BiOCl, fine observation showed that the catalyst doped with Fe element, The looser stacking density and the smaller diameter and larger surface area of the cake structure can provide more active sites for the reaction and improve the catalytic activity of the photocatalyst. On the whole, the BiOCl and Fe-BOC-3 photocatalysts showed uniform nanorapelike structure, and the structure size and distribution were basically consistent. Figure 3(e) analysis results show that the prepared Fe-BOC-3 exhibits a similar circular cake structure, which is consistent with the results observed in SEM. It can be seen from Fig. 3(f)

that the lattice fringe spacing of 0.275 nm corresponds to the (110) crystal plane of tetragonal BiOCl (Mi et al. 2016). The crystal lattice fringe and edge of Fe-BOC-3 composite photocatalyst are clear, and there is no amorphous state, indicating that the prepared Fe-BOC-3 composite catalyst presents a highly crystalline state. Iron doping does not change the structure, particle size and morphology of BiOCl on a single catalyst. Due to the low iron loading and highly dispersed distribution in Fe-BOC-3 composite catalyst, this phenomenon indicates that Fe doping has almost no effect on BiOCl cuboid structure. In order to further verify whether iron element is highly dispersed within the catalyst, the catalyst was characterized by EDS-Mapping. Figure 3(g) shows the scanning capture area of EDS-Mapping. Fig. S1 shows that the main elements in Fe-BOC-3 catalyst sample are Bi, O and Cl. In addition, the presence of Fe suggests that the element was successfully doped into the BOC structure. Figure 3(g, h, i, j, k, l) shows the scanning diagram and individual distribution of elements in Bi, Fe, O and Cl of Fe-BOC-3 catalyst samples respectively. All these confirm that iron element is indeed dispersed in Fe-BOC-3 composite catalyst, and the distribution is uniform and dispersed, which is consistent with the above XRD, SEM and HR-TEM analysis results.

3.3 Specific surface area analysis

The photocatalytic activity of a photocatalyst is strongly bound up with the corresponding specific surface area. The N₂ adsorption-desorption isotherms and pore size distribution curves of BOC and Fe-BOC-3 were shown in Fig. 4 and Table S1, as shown in Fig. 4 (a) and 4 (c), it can be clearly seen that the adsorption capacity of BOC and Fe-BOC-3 photocatalysts in the low relative pressure (p/p_0) region is small, and there is no obvious inflection point in the figure, the adsorption capacity increases significantly with the increase of relative pressure, indicating that both BOC and Fe-BOC-3 photocatalysts are type III adsorption isotherms. At the same time, when the catalyst is in the desorption state, both BOC and Fe-BOC-3 catalysts show H3 hysteresis (Chang et al. 2014), which indicates that BOC and Fe-BOC-3 photocatalysts have a mesoporous structure formed by the stacking of cracked and nano sheets (Cao et al. 2012, Xiang et al. 2011). Through further analysis of the pore size distribution curve of the catalyst, it is found that the pore size of BOC and Fe-BOC-3 catalysts is mainly distributed between 7–40 nm, which further proves that the pore size of BOC and Fe-BOC-3 catalysts is mesoporous. Table 2 lists the specific surface area, pore diameter and pore volume values of all different photocatalysts. It is obvious that the specific surface area and pore volume of the catalyst increase with the increase of Fe doping, but the pore size does not change significantly.

Table 1
BET and pore size of different catalysts

Photocatalyst	specific surface area (m ² /g)	aperture (nm)	pore volume (cm ³ /g)
BiOCl	29.448	17.26	0.167
Fe-BOC-3	35.835	17.29	0.207

Curve(b,d) of BOC and Fe-BiOCl-3

3.4 XPS analysis

In order to judge the main surface element types, valence states and chemical compositions of the catalyst samples, the Fe-BOC-3 catalyst samples were characterized and analyzed by XPS. In the full spectrum shown in Fig. 5 (a), it can be observed that Fe-BOC-3 catalyst has characteristic absorption peaks of major elements Bi, O, Cl and Fe. Figure 5(b) is the XPS spectrum of Bi 4f of Fe-BOC-3. It shows that there are two characteristic absorption peaks at the binding energies of 158.08 and 163.38 eV, which respectively correspond to Bi 4f_{7/2} and Bi 4f_{5/2} of Bi³⁺, indicating that the chemical valence of Bi element in Fe-BOC-3 catalyst is positive trivalent (Mi et al. 2016, Sun et al. 2019a, Wang et al. 2019). Figure 5 (c) is the XPS spectrum of Cl 2p of Fe-BOC-3, showing two characteristic absorption peaks. The main peaks at the binding energies of 196.78 and 198.38 eV can correspond to Cl 2p_{3/2} and Cl 2p_{1/2} respectively. Figure 5(d) is the XPS spectrum of O 1s of Fe-BOC-3, in which the fitted binding energy is the characteristic absorption peak of 528.78 eV, belonging to the Bi-O bond of Fe-BOC-3; The characteristic absorption peak with a binding energy of 530.18 eV corresponds to the C-O bond on the catalyst surface; the characteristic absorption peak with binding energy of 531.88 eV should be attributed to oxygen vacancy (Zhong et al. 2020). Relatively speaking, the peak at the binding energy of 531.88 eV is weak, indicating that the content of oxygen vacancy is low. Figure 5(e) shows the XPS spectrum of Fe in Fe-BOC-3. The absorption peak of element Fe can be seen at the binding energy of 710 eV, which indicates that iron exists in the form of iron oxygen bond, but this peak is very weak, indicating that the content is very low, which is consistent with the low content of oxygen vacancy.

3.5 UV-vis DRS analysis

In order to explore the optical absorption properties of different catalyst samples, the catalyst samples were tested and analyzed by UV visible diffuse reflectance absorption spectroscopy. The ultraviolet visible absorption spectra of BOC, Fe-BOC-1, Fe-BOC-2, Fe-BOC-3 and Fe-BOC-4 are shown in Fig. 6. As shown in Fig. 6 (a), BOC has strong optical absorption performance between 200–350 nm. With the addition of Fe element, the absorption edges of Fe-BOC-1, Fe-BOC-2, Fe-BOC-3 and Fe-BOC-4 are significantly red shifted relative to BOC, and the Fe-BOC-1, Fe-BOC-2, Fe-BOC-3 and Fe-BOC-4 catalysts have obvious absorption peaks in the region of 350–550 nm. With the increase of iron element doping, the UV visible absorption capacity is gradually enhanced, it is speculated that the introduction of Fe may increase the adsorption performance of the composite catalyst samples under visible light driving. The absorption curves of Fe-BOC-3 and Fe-BOC-4 catalysts are basically the same, and the absorption sidebands are all around 550 nm, indicating that the adsorption capacity of visible light has reached the limit.

As shown in Fig. 6 (b), the band gap of catalyst samples BOC, Fe-BOC-1, Fe-BOC-2, Fe-BOC-3 and Fe-BOC-4 is calculated according to the following formula:

$$A(h\nu - E_g)^{n/2} = \alpha h\nu$$

The band gap values of BOC, Fe-BOC-1, Fe-BOC-2, Fe-BOC-3 and Fe-BOC-4 catalyst samples were calculated to be 3.24, 3.20, 3.03, 2.69 and 2.66 eV respectively. This result shows that with the gradual increase of Fe doping amount, the modification of single catalyst BOC by Fe doping can significantly change the band gap width of BOC, and generate new doping energy levels in the band gap of BOC. The light absorption region of Fe-BOC-1, Fe-BOC-2, Fe-BOC-3 and Fe-BOC-4 catalysts is extended to the visible region, showing low band gap energy, thus improving the photocatalytic oxidation capacity (Guo et al. 2020, Peng et al. 2021, Tian et al. 2019). Table S2 lists the absorption edge and band gap values for different catalysts.

3.6 Photocatalytic degradation of CIP

The performance of photocatalyst prepared by one-step hydrothermal synthesis for CIP degradation was investigated. The doping of iron element will significantly change the band gap of BiOCl photocatalyst, thus affecting the response range of photocatalyst under visible light, achieving the absorption capacity of visible light in different ranges, thus affecting the catalytic activity of photocatalyst. It is necessary to investigate the doping amount of Fe in BOC photocatalyst because the doping of Fe with different content in the crystal structure of BiOCl is not positively correlated with its ability to change the UV-Vis absorption light and the band gap width. The conditions of photocatalysis experiment are: initial concentration of CIP 10 mg/L, catalyst dosage 0.6 g/L, pH value 5.8, temperature 25 ± 2 °C. The degradation effect and kinetics of CIP degradation by BiOCl, Fe-BOC-1, Fe-BOC-2, Fe-BOC-3 and Fe-BOC-4 photocatalysts prepared in the experiment are shown in Fig. 7.

As shown in Fig. 7 (a), the removal rate of CIP by BOC is 33.8%. With the increase of Fe doping, the removal rates of CIP by Fe-BOC-1, Fe-BOC-2, Fe-BOC-3 and Fe-BOC-4 are 40.0%, 36.4%, 42.6% and 38.1% respectively. The results showed that Fe doping changed the degradation activity of BOC catalyst. Even though the doping ratio was different, the degradation effect of BOC catalyst was higher than that of BOC catalyst for CIP. Among them, Fe-BOC-3 has the best degradation effect, which may be because Fe doping increases the active sites of the catalyst and reduces the recombination rate of holes and electrons, thus improving the catalytic performance of the photocatalyst. The degradation activity of Fe doped catalyst is obviously better than that of undoped catalyst. The different content of Fe doped catalyst will also affect the activity of the catalyst, which may be related to the specific surface area of the synthesized catalyst. In Fig. 7 (b), there is a linear relationship between photocatalytic reaction time and CIP degradation rate, which basically conforms to the quasi first-order kinetic equation. According to the analysis and calculation of Langmuir-H kinetic model, the quasi first-order kinetic equation of CIP degradation by five photocatalysts and the R^2 value of the reaction are obtained (Table S3). It can be seen from Table S3 that the degradation of CIP by the five photocatalysts is more in line with the first-order kinetics. The degradation rate constant of CIP by Fe-BOC-3 is 0.0058 min^{-1} , which is higher than the reaction rate of single catalyst BiOCl, Fe-BOC-1, Fe-BOC-2, Fe-BOC-3 and Fe-BOC-4. The reaction

degradation rate of Fe doped photocatalyst is higher than that of single catalyst, which indicates that Fe doped photocatalyst can improve the degradation rate of CIP.

3.7 Degradation of CIP by persulfate activated by BiOCl and Fe-BOC

After investigating the effects of different catalysts prepared in the experiment on CIP degradation, the effects of different catalysts prepared on CIP degradation by activated persulfate were further explored. The effects of activated persulfate on CIP removal efficiency of BOC, Fe-BOC-1, Fe-BOC-2, Fe-BOC-3 and Fe-BOC-4 catalysts under simulated visible light were investigated. The conditions of photocatalysis experiment are: initial concentration of CIP 10 mg/L, catalyst dosage 0.6 g/L, persulfate concentration 1 mM, pH value 5.8, temperature 25 ± 2 °C. The degradation effect and kinetics of activated persulfate for CIP degradation by the photocatalyst prepared in the experiment are shown in Fig. 8.

As shown in Fig. 8 (a), under the simulated visible light conditions, the removal rate of CIP by BOC/PS is 49.8%; With the increase of iron doping, the removal rates of CIP by Fe-BOC-1/PS, Fe-BOC-2/PS, Fe-BOC-3/PS and Fe-BOC-4/PS were 59.9%, 54.0%, 81.4% and 60.9% respectively. The analysis results show that the degradation effect of activated persulfate catalyst on CIP is significantly higher than that of a single catalyst. With the doping of iron, the removal effect of Fe-BOC photocatalyst on CIP is increased to a certain extent compared with that of pure BOC photocatalyst. Among them, the degradation effect of Fe-BOC-3/PS on CIP is about 31.6% higher than that of BOC/PS, and nearly double that of Fe-BOC-3 catalyst. Obviously, Fe-BOC-3/PS has the best catalytic performance. This phenomenon shows that Fe-BOC-3 catalyst can significantly improve the activity of persulfate, promote the decomposition of persulfate to produce free radicals to participate in the reaction, and then improve the removal rate of CIP. In Fig. 8 (b), there is a linear relationship between photocatalytic reaction time and CIP degradation rate, which basically conforms to the quasi first-order kinetic equation. According to Table S4, the reaction rate constant of single catalyst BiOCl/PS is 0.0068 min^{-1} , and Fe-BOC-3/PS is increased to 0.0172 min^{-1} , which is superior to the other three systems, indicating that Fe-BOC-3/PS system significantly improves the degradation rate of CIP.

3.8 Dosage of Fe-BOC-3 catalyst for CIP degradation

The dosage of catalyst is also an important influence on the degradation effect. Five kinds of Fe-BOC-3 dosage of 0.2 g/L, 0.4 g/L, 0.6 g/L, 0.8 g/L and 1.0 g/L were selected in the experiment. The best dosage of catalyst was determined by observing the influence on CIP removal effect. The conditions of photocatalysis experiment are as follows: initial concentration of CIP is 10 mg/L, persulfate concentration is 1 mM, and pH value is 5.8, Temperature 25 ± 2 °C. The degradation effect and kinetics of CIP degradation with different dosage of catalyst are shown in Fig. 9.

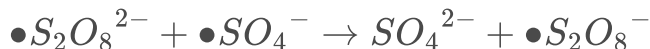
As shown in Fig. 9 (a), when the dosage of catalyst increases from 0.2 g/L to 1.0 g/L, the removal rates of CIP are 37.2%, 60.6%, 81.4%, 78.9% and 75.1% respectively, and the degradation effect shows a trend of first increasing and then decreasing. The results show that when the catalyst dosage is 0.6 g/L, the CIP

removal effect is the best, and the CIP removal rate is 81.4% within 90 minutes. This may be because the increase of the catalyst dosage provides more reaction sites and produces more free radicals. However, when the dosage of catalyst increases to 1.0 g/L, the removal rate of CIP shows a downward trend. It may be that excessive catalyst will weaken the light transmittance, which becomes an obstacle to visible light scattering, resulting in the reduction of the production of free radicals and photogenerated electrons in the system, thus making the degradation effect worse. Therefore, the catalyst dosage of 0.6 g/L was selected as the optimal dosage for the experiment. In Fig. 9 (b), there is a linear relationship between photocatalytic reaction time and CIP degradation rate, which basically conforms to the quasi first-order kinetic equation. According to the analysis and calculation of Langmuir-H kinetic model, the quasi first-order kinetic equation of CIP degradation with different dosage and the R^2 value of the reaction are obtained (Table S5). The R^2 of the dosage of the above five Fe-BOC-3 photocatalysts are close to 1, indicating that there is a good correlation between CIP degradation rate and reaction time. According to Table S5, the degradation rate constant of CIP by Fe-BOC-3 with the highest reaction rate constant of 0.6 g/L dosage is 0.0172 min^{-1} , indicating that the degradation rate of CIP by 0.6 g/L dosage is significantly higher than that by other dosage catalysts.

3.9 Degradation of CIP by persulfate dosing concentration

Persulfate in the whole system can be activated by visible light and catalyst to produce active oxides to participate in the degradation process of CIP. Five persulfate concentrations of 0.5 mM, 0.8 mM, 1.0 mM, 1.2 mM and 1.5 mM were selected in the experiment. The best persulfate concentration was determined by observing the impact on CIP removal effect. The conditions of photocatalysis experiment are as follows: initial concentration of CIP is 10 mg/L catalyst dosage is 0.6 g/L, and pH value is 5.8. Temperature $25 \pm 2 \text{ }^\circ\text{C}$. In Fig. 10 for degradation effect and kinetics of CIP degraded by persulfate dosing concentration.

As shown in Fig. 10 (a), as the dosage of persulfate increases from 0.5 mM to 1.5 mM, the CIP removal rates are 72.0%, 75.3%, 81.4%, 71.0% and 66.8%. With the gradual increase of persulfate concentration, the removal effect of persulfate on CIP increased first and then decreased. When the concentration of persulfate was 1 mM, the CIP removal rate reached 81.4% after 90 min. However, when the concentration of persulfate in the solution is increased to 1.5 mM, the removal rate of CIP decreases by 14.6%. This result may be because the reaction between sulfate radical generates sulfate ion, which loses the oxidation ability. On the other hand, the side reaction between excessive sulfate and radical will also compete with the degradation of CIP, thus affecting the removal rate of CIP. Formula (5)–(8) for the reaction equation. Therefore, persulfate with a concentration of 1 mM was selected as the best concentration of PS in the experiment to participate in the reaction. $\bullet\text{SO}_4^- + \bullet\text{SO}_4^- \rightarrow 2 \bullet\text{SO}_4^-$ (5)



6



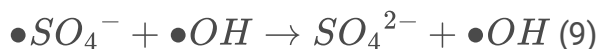


By analyzing Fig. 10(b), it can be clearly seen that there is an obvious linear relationship between the photocatalytic time of the reaction and the CIP degradation rate, which basically conforms to the quasi first-order kinetic equation. Based on the analysis and calculation of Langmuir-H kinetic model, the quasi first-order kinetic equation of photocatalytic degradation of CIP with five different PS concentrations and the R^2 of the reaction are obtained (Table S6). The R^2 of the above five different persulfate initial dosing concentrations are close to 1, indicating that there is a good correlation between CIP degradation rate and reaction time. It can be seen from the Table S6 that there is a good correlation between CIP degradation rate and reaction time. When the concentration of persulfate is 1.0 mM, the degradation reaction rate of CIP in the system is higher than that of other persulfate dosing concentrations. The reaction rate constant is 0.0172 min^{-1} , indicating that when the concentration of persulfate is 1.0 mM, the degradation rate of CIP is the fastest and the degradation effect is the best, and the persulfate in the system shows the best oxidation.

3.10 Degradation of CIP by pH

In addition to the above influence conditions, the influence of the initial pH value of the solution on the degradation effect of CIP in the whole degradation system was investigated. The pH range of the experiment was 3.0–11.0, which were pH = 3, 5.8, 7, 9 and 11 respectively. pH value is 5.8 means that the pH value of ciprofloxacin solution itself has not been adjusted by acid and alkali. The initial pH value was determined by the influence on the CIP removal effect under different pH values. The conditions of photocatalysis experiment are: initial concentration of CIP 10 mg/L, catalyst dosage 0.6 g/L, persulfate concentration 1 mM, temperature $25 \pm 2 \text{ }^\circ\text{C}$. The degradation effect and kinetics of CIP degradation with different dosage of catalyst are shown in Fig. 11.

As shown in Fig. 11 (a), the degradation effect of CIP in acidic solution is better than that in alkaline solution. With the pH from 3.0 to 7.0, the degradation effect of CIP gradually increased, and the removal effect of CIP began to decline when the pH was 9.0. When it reaches 11.0, it drops further. This phenomenon is because persulfate becomes more stable under acidic conditions, and persulfate can be activated into more sulfate radicals in the reaction, thus promoting the degradation of CIP; Under alkaline conditions, sulfate radical can be converted into hydroxyl radical. Compared with sulfate radical, the oxidation-reduction potential of hydroxyl radical is lower and the oxidation capacity is weaker, which will also reduce the removal rate of CIP. The reaction equations are (9) and (10). Therefore, in the whole experimental reaction system, the pH value is not adjusted to degrade CIP under natural pH value.

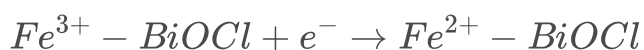


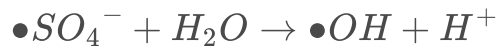
In Fig. 11 (b), there is a linear relationship between photocatalytic reaction time and CIP degradation rate, which basically conforms to the quasi first-order kinetic equation. According to the analysis and calculation of the Langmuir-H kinetic model, the quasi first-order kinetic equations of the reactions with different pH values and the R^2 of the reactions are obtained (Table S7). The R^2 values of the five reaction conditions with different pH values are close to 1, indicating that there is a good correlation between the CIP degradation rate and the reaction time according to Table S7. The analysis shows that when pH is 3 and 5.7, the degradation effect of CIP in the reaction system is similar. When pH is 5.7, the reaction rate constant of the system is 0.0172, which is higher than the reaction rate constant of 0.0165 when pH is 3, indicating that when pH is 5.7 in the system. The degradation rate constant of the whole reaction is the highest, and the degradation rate of CIP is higher, showing a good catalysis.

3.11 Degradation of CIP in different systems

After determining the single influencing factor, in order to further explore the effect of different combination systems on CIP degradation, the optimal degradation system was further determined. The effects of six different systems PS, Fe-BOC-3, Vis/PS, Vis/Fe-BOC-3, Fe-BOC-3/PS and Vis/Fe-BOC-3/PS on CIP removal efficiency were investigated. The conditions of photocatalysis experiment are: initial concentration of CIP 10 mg/L, catalyst dosage 0.6 g/L, persulfate concentration 1 mM, pH value 5.8, temperature 25 ± 2 °C. The degradation effect and reaction rate of CIP degradation by different combination systems are shown in Fig. 12.

It can be seen from Fig. 12(a) that the individual persulfate system has little degradation effect on CIP; The Fe-BOC-3 photocatalyst alone can only adsorb 13.5% CIP under dark conditions, and basically reaches the adsorption peak at 45 min. the adsorption capacity of the Fe-BOC-3 photocatalyst alone to CIP can be neglected when the time lasts to 90 min. Because light can activate persulfate, the removal rate of CIP in Vis/PS system is 9.6% higher than that of PS alone. In the simulated visible light activated Fe-BOC-3 system, the degradation and removal rate of CIP was 42.6%. In the catalyst fe-boc-3 activated PS system, the degradation and removal rate of CIP was 57.9%. Compared with other systems, the removal rate of CIP in Vis/Fe-BOC-3/PS system increased significantly, and the removal rate was 81.4%. This is due to the presence of Fe^{2+} and Fe^{3+} in Fe doped BOC catalyst. iron element can activate persulfate and generate $\bullet SO_4^-$ and $\bullet OH$, under the irradiation of visible light. During the degradation process under this system, active oxides can be generated cyclically through catalytic reaction. the following equation for the cyclic reaction:





In Fig. 12 (b), the reaction rate constants of Fe-BOC-3, Vis/PS, Vis/Fe-BOC-3, Fe-BOC-3/PS and Vis/Fe-BOC-3/PS systems are 0.00157, 0.00103, 0.0058, 0.0087 and 0.0172 min^{-1} respectively. After adding persulfate to Fe-BOC-3, the degradation rate constant of CIP is increased by nearly three times, indicating that Fe-BOC-3 photocatalyst can effectively activate persulfate, thus improving the degradation rate of CIP.

3.12 Stability of photocatalyst

The purpose of this experiment is to investigate whether the Fe-BOC-3 photocatalyst has good repeatability. Four cycle experiments are set to evaluate the cycle ability of Fe-BOC-3 photocatalyst through the change of CIP degradation effect. The removal rate of CIP in the four cycle experiment is shown in Fig. 13, after each cycle of Fe-BOC-3, CIP was still effectively degraded. The results of the fourth cycle showed that the removal rate of CIP could still reach 76%. It shows that the prepared Fe-BOC-3 can still activate persulfate to degrade CIP efficiently after four cycles, which proves that the Fe-BOC-3 photocatalyst has high stability and provides a basic idea for future practical application.

3.13 Bioacute toxicity analysis of ciprofloxacin degradation products

Ciprofloxacin will produce some new by-products in the degradation process, which may have higher biological toxicity than ciprofloxacin itself. Therefore, it is necessary to study the changes of biological acute toxicity before and after ciprofloxacin degradation. The photoinhibition rate of *Vibrio Fischeri* was used to evaluate the photoinhibition of 10 mg/L ciprofloxacin at 0, 30, 60 and 90 min. The acute toxicity test results of luminescent bacteria are shown in Fig. 14. With the reaction time, the cytotoxicity of *Vibrio Fischeri* gradually lost and the relative inhibition rate gradually decreased. When the reaction time reached 90 min, the relative inhibition rate of ciprofloxacin decreased from 55.67–46.83%. The results showed that the biological toxicity of ciprofloxacin solution was further reduced after degradation in Vis/Fe-BOC-3/PS system, which proved that there was no more toxic degradation product in the degradation process of Vis/Fe-BOC-3/PS system. The toxicity after degradation is the residual toxicity of intermediate products after degradation. The test method of luminescent bacteria is only an evaluation method for detecting the acute toxicity of organisms, and other toxicity of ciprofloxacin needs to be further explored.

3.14 Identification and analysis of reactive substances in catalytic system

In the process of photocatalytic reaction, a variety of active substances will be produced to participate in oxidation. The most common active substances are holes (h^+), superoxide radicals ($\bullet O_2^-$) and hydroxyl radicals ($\bullet OH$), while activated persulfate usually produces sulfate radicals ($\bullet SO_4^-$) to

participate in the reaction. In order to explore which active substances play a role in the degradation of ciprofloxacin by Vis/Fe-BOC-3/PS composite photocatalyst system, free radical capture experiment and EPR detection technology were set up to identify and analyze the types of active groups in the reaction. In the free radical capture experiment, methanol (MeOH) simultaneously captures ($\bullet OH$) and ($\bullet SO_4^-$), tertiary butyl alcohol (TBA) captures $\bullet OH$, ammonium oxalate (AO) captures h^+ , and p-benzoquinone (BQ) captures $\bullet O_2^-$ (Liu et al. 2021d, Tahmasebi et al. 2019). The inhibition of CIP degradation was investigated when the molar ratio of methanol, tert butyl alcohol, ammonium oxalate to persulfate concentration was 5:1 and the molar ratio of p-benzoquinone to persulfate concentration was 0.5:1. The removal effect of CIP obtained by adding different capture agents in Vis/Fe-BOC-3/PS system is shown in Fig. 15.

Figure 15 shows that in the Vis/Fe-BOC-3/PS without any capture agent, the removal rate of CIP is 81.4%; When 5 mM methanol was added to the system to capture $\bullet OH$ and $\bullet SO_4^-$ in the reaction, the removal rate of CIP decreased to 72.7%; When 5 mm tert butyl alcohol to capture $\bullet OH$ in the reaction, the removal rate of CIP decreased to 74.5%; When 5 mM ammonium oxalate to capture h^+ , the removal rate of CIP decreased to 80.3%;

When 0.5 mM of P-benzoquinone to capture $\bullet O_2^-$, the removal rate of CIP decreased to 78.9%. It shows that in the Vis/Fe-BOC-3/PS reaction system, methanol, tert butyl alcohol and P-benzoquinone have inhibitory effects on the degradation of CIP, while the inhibitory effect of ammonium oxalate is not obvious, which proves that there are active oxidizing substances in the reaction system for the degradation of CIP, among which $\bullet OH$, $\bullet SO_4^-$ and $\bullet O_2^-$ have more obvious inhibitory effects on the removal rate of CIP and occupy a more important dominant position. To further clarify the existence of free radicals in the reaction system, the three active substances that play a leading role in the reaction system were detected and analyzed by EPR capture technology. Different from the free radical capture experiment, $\bullet OH$ and $\bullet SO_4^-$ were captured in ultra pure water; $\bullet O_2^-$ is captured in methanol solution (Wu et al. 2022). EPR spectra of $\bullet OH$, $\bullet SO_4^-$ and $\bullet O_2^-$ are shown in Fig. 16.

As shown in Fig. 16 (a), after 15 min of illumination, the characteristic signals of $DMPO - \bullet OH$ adduct and $DMPO - \bullet SO_4^-$ adduct appeared in the EPR spectrum, indicating the presence of $\bullet OH$ and $\bullet SO_4^-$ in the Vis/Fe-BOC-3/PS system. The signal intensity shown in the EPR spectrum is significantly higher than that of, which indicates that the dominant role in the reaction system is stronger than that of, which is consistent with the results of the free radical capture experiment. The EPR spectrum shows that the signal intensity of $\bullet OH$ is significantly higher than that of $\bullet SO_4^-$, which indicates that the dominant role of $\bullet OH$ in the reaction system is stronger than that of $\bullet SO_4^-$, which is consistent with the results of free radical capture experiment. The weak characteristic signal of $DMPO - \bullet SO_4^-$ adduct may be due to the fact that the selected EPR detection time is 15 min after illumination, when the free radicals are consumed more by pollutants;

In addition, $\bullet SO_4^-$ will be rapidly converted to $\bullet OH$ in the reaction system, making the characteristic signal in the EPR spectrum weak (Liu et al. 2021c). As shown in Fig. 3–19 (b), the characteristic signal

peak of O₂ appears in the EPR spectrum after 15 min of illumination (Jia et al. 2020). These results showed that active substances such as $\bullet OH$, $\bullet SO_4^-$ and $\bullet O_2^-$ were involved in the degradation of CIP in the photocatalytic process.

3.15 Degradation pathways of CIP

Intermediate products will be produced in the process of degrading ciprofloxacin, and some intermediate products may be more toxic than ciprofloxacin. Therefore, it is particularly important to identify the intermediate products produced during the degradation of ciprofloxacin. In this study, liquid chromatography-mass spectrometry (LC-MS) was used to identify the possible intermediates of ciprofloxacin ($m/z = 332$) in the photodegradation reaction of Vis/Fe-BOC-3/PS system. See Table 3 for the intermediates. In addition, the main intermediates with m/z of 362, 334 and 263 were analyzed by secondary mass spectrometry (Fig. S2-S11 for the primary and secondary mass spectra of intermediates).

For the intermediate compound with parent ion m/z of 362, there are sub ion fragments with m/z of 344 in the second-order mass spectrum. It is speculated that the fragments may be formed due to the loss of H₂O from the parent ion; For the parent ion with m/z of 334, there are sub ion fragments with m/z of 316 in the secondary mass spectrum, which is speculated to be formed by the loss of H₂O from the parent ion; For the parent ion with m/z of 263, there are sub ion fragments with m/z of 245 in the secondary mass spectrum. It is speculated that the fragments may be formed due to the loss of H₂O from the parent ion.

In addition, according to previous research reports, the degradation of CIP is mainly through piperazine ring breakage, fluorine substitution and carbonylation reactions (Hu et al. 2021, Liang et al. 2021, Liu et al. 2021b, Yang et al. 2021). Therefore, two possible degradation pathways of CIP are proposed in combination with the mass spectrogram, and the degradation path diagram is shown in Fig. 17.

The degradation path 1: m/z 362 may be due to the ring opening of piperazine to form aldehyde(-CHO) compounds; m/z 334 may be formed by decarbonylation of m/z 362 compounds; m/z 306 may be formed by the loss of carbonyl group of m/z 334 compound to form a de vinyl compound (An et al. 2010); m/z 291 compound is formed by loss of N atom and oxidation to ketone group; m/z 263 is the product of further decarbonylation reaction. At this time, the piperazine ring of ciprofloxacin is completely destroyed.

The degradation path 2: m/z 346 may be a compound formed after defluorination and hydroxylation of CIP; m/z 301 compound may be the product of decarboxylation of m/z 346 compound (Zhu et al. 2021).

Therefore, the main degradation pathway of CIP is that the piperazine ring in CIP molecule has high electron density and is mainly attacked by various free radicals. The main reactions include piperazine ring opening, decarbonylation, decarboxylation and fluorine substitution.

Table 2
Intermediate products of ciprofloxacin degradation

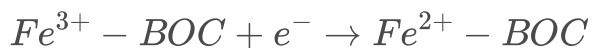
m/z	Molecular formula	Structure diagram
332	C ₁₇ H ₁₈ FN ₃ O ₃	
362	C ₁₇ H ₁₆ FN ₃ O ₅	
334	C ₁₆ H ₁₆ FN ₃ O ₄	
306	C ₁₅ H ₁₆ FN ₃ O ₃	
291	C ₁₄ H ₁₂ FN ₂ O ₄	
263	C ₁₃ H ₁₂ FN ₂ O ₃	
346	C ₁₇ H ₁₆ FN ₃ O ₄	
301	C ₁₆ H ₁₅ FN ₃ O ₂	

3.16 Mechanism of Vis/Fe-BOC-3/PS system

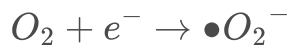
The degradation mechanism of Vis/Fe-BOC-3/PS in the system was deduced from free radical trapping experiment and EPR analysis. Under the irradiation of simulated visible light, the doping of iron element promotes the conversion from UV region to visible region, and the conversion between Fe³⁺ and Fe²⁺ occurs in this process; In addition, Fe³⁺ can activate PS to generate •OH and •SO₄⁻. As the transition of electrons will produce corresponding holes, Fe-BOC-3 reacts with H₂O and O₂ to produce active substances. Formulas (14)–(19) for the reaction equation.



14



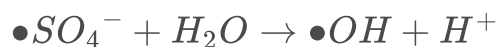
15



16



17



18



19

4. Conclusions

In summary, the single catalyst BiOCl and Fe-BiOCl photocatalysts doped with different iron elements were prepared by one-step hydrothermal synthesis. Compared with the original BiOCl, the prepared Fe BOC photocatalyst showed significant performance in the degradation of CIP under xenon lamp. Iron doping can enlarge the surface area of Fe-BOC-X material, improve the adsorption capacity, and provide rich photocatalytic active sites for the decomposition of organic pollutants. BiOCl is mainly concentrated in the ultraviolet absorption region, and after Fe doping, the optical absorption region is extended to the visible light range, effectively improving the light response range; the band gap energies of BiOCl, Fe-BOC-1, Fe-BOC-2, Fe-BOC-3 and Fe-BOC-4 are 3.24, 3.20, 3.03, 2.69 and 2.66 eV, which is conducive to reducing the electron hole recombination rate and effectively improving the ability to activate persulfate; Fe-BOC-3 is the photocatalyst with the best doping ratio. Under the best conditions (pH = 5.7, PS = 1.0 mm, Fe-BOC = 0.6 g/L, CIP = 10mg/l), the removal rate of ciprofloxacin by Vis/Fe-BOC-3/PS system is 81.4%; The results of free radical trapping experiment and EPR detection showed that in the Vis/Fe-BOC-3/PS system, $\bullet OH$, $\bullet SO_4^-$, h^+ and $\bullet O_2^-$ and were involved in the photocatalytic reaction to varying degrees, in which, $\bullet OH$, $\bullet SO_4^-$ active oxidizing substances were dominant; through mass spectrometry analysis, it is found that the main degradation pathway of CIP is the process that the piperazine ring in CIP molecule is attacked by various free radicals to produce a series of other products. The main reaction processes include piperazine ring opening, decarbonylation, decarboxylation and fluorine substitution. In addition, in the process of photocatalysis, the acute toxicity of organisms is reduced, which indicates that Fe-BOC-X has great practical application potential in the further treatment of quinolone antibiotic wastewater. Since the synergistic effect between photocatalysis and PS is a promising and effective pollutant degradation strategy, this work will stimulate people's interest in the construction of Vis/Fe-BOC-X/PS photocatalyst for photocatalytic degradation in the presence of PS.

Declarations

Declarations

The authors declare that they have no known competing financial interests or personal relationships that could have appeared to influence the work reported in this paper.

Ethics approval and consent to participate

Not applicable

Consent for publication

Not applicable

Declarations

Competing interests

The authors declare that they have no competing interests

Funding

Our work was supported by the National Natural Science Foundation of China (Grant No. 51778267), the National Water Pollution Control and Treatment Science and Technology Major Project (No. 2012ZX07408001), the Jilin Province Science and Technology Department Project (No. 20190201113JC), the Jilin Provincial Department of Ecology and Environment Project (No.2019-15).

Authors' contributions

Gen Liu: writing, Methodology, Yingzi Lin: funding support, reviewing, Siwen Li: Methodology, Chunyan Shi: Methodology, Dongyan Zhang: Methodology, Lei Chen: Methodology.

References

1. Adhikari S, Kim DH (2018) Influence of surfactant on the synthesis of BiOCl/WO₃ microcomposites for enhanced adsorption in aqueous solutions. *Korean J Chem Eng* 36:468–477
2. An T, Yang H, Li G, Song W, Cooper WJ, Nie X (2010) Kinetics and mechanism of advanced oxidation processes (AOPs) in degradation of ciprofloxacin in water. *Appl Catal B* 94:288–294
3. Cao J, Xu B, Lin H, Luo B, Chen S (2012) Chemical etching preparation of BiOI/BiOBr heterostructures with enhanced photocatalytic properties for organic dye removal. *Chem Eng J* 185–186:91–99
4. Carpio IEM, Ansari A, Rodrigues DF (2018) Relationship of Biodiversity with Heavy Metal Tolerance and Sorption Capacity: A Meta-Analysis Approach. *Environ Sci Technol* 52:184–194
5. Castrignano E, Kannan AM, Proctor K, Petrie B, Hodgen S, Feil EJ, Lewis SE, Lopardo L, Camacho-Munoz D, Rice J, Cartwright N, Barden R, Kasprzyk-Hordern B (2020) (Fluoro)quinolones and quinolone resistance genes in the aquatic environment: A river catchment perspective. *Water Res* 182:116015
6. Chang F, Xie Y, Zhang J, Chen J, Li C, Wang J, Luo J, Deng B, Hu X (2014) : Construction of exfoliated g-C₃N₄ nanosheets–BiOCl hybrids with enhanced photocatalytic performance. *RSC Advances* 4
7. Chen L, Ni R, Yuan T, Gao Y, Kong W, Zhang P, Yue Q, Gao B (2020) Effects of green synthesis, magnetization, and regeneration on ciprofloxacin removal by bimetallic nZVI/Cu composites and

- insights of degradation mechanism. *J Hazard Mater* 382:121008
8. Chen MM, Niu HY, Niu CG, Guo H, Liang S, Yang YY (2022) Metal-organic framework-derived CuCo/carbon as an efficient magnetic heterogeneous catalyst for persulfate activation and ciprofloxacin degradation. *J Hazard Mater* 424:127196
 9. Di J, Xia J, Ji M, Wang B, Yin S, Zhang Q, Chen Z, Li H (2015) Carbon Quantum Dots Modified BiOCl Ultrathin Nanosheets with Enhanced Molecular Oxygen Activation Ability for Broad Spectrum Photocatalytic Properties and Mechanism Insight. *ACS Appl Mater Interfaces* 7:20111–20123
 10. Dominguez CM, Rodriguez V, Montero E, Romero A, Santos A (2020) : Abatement of dichloromethane using persulfate activated by alkali: A kinetic study. *Separation and Purification Technology* 241
 11. Fan X, Ding S, Chen M, Gao S, Fu Z, Gong M, Tsang DCW, Wang Y, Zhang C (2019) Peak Chromium Pollution in Summer and Winter Caused by High Mobility of Chromium in Sediment of a Eutrophic Lake: In Situ Evidence from High Spatiotemporal Sampling. *Environ Sci Technol* 53:4755–4764
 12. Feiteiro J, Mariana M, Cairrao E (2021) Health toxicity effects of brominated flame retardants: From environmental to human exposure. *Environ Pollut* 285:117475
 13. Fernandes A, Makoś P, Boczkaj G (2018) Treatment of bitumen post oxidative effluents by sulfate radicals based advanced oxidation processes (S-AOPs) under alkaline pH conditions. *J Clean Prod* 195:374–384
 14. Gao YQ, Gao NY, Chu WH, Zhang YF, Zhang J, Yin DQ (2019) UV-activated persulfate oxidation of sulfamethoxypyridazine: Kinetics, degradation pathways and impact on DBP formation during subsequent chlorination. *Chem Eng J* 370:706–715
 15. Ghanbari F, Moradi M (2017) Application of peroxymonosulfate and its activation methods for degradation of environmental organic pollutants: Review. *Chem Eng J* 310:41–62
 16. Githinji LJM, Musey MK, Ankumah RO (2010) Evaluation of the Fate of Ciprofloxacin and Amoxicillin in Domestic Wastewater. *Water Air Soil Pollut* 219:191–201
 17. Gu Y-y, Zhao L, Yang M-y, Xiong Y-q, Wu Z, Zhou M-j, Yan J (2017) Preparation and characterization of highly photocatalytic active hierarchical BiOX (X = Cl, Br, I) microflowers for rhodamine B degradation with kinetic modelling studies. *J Cent South Univ* 24:754–765
 18. Guellati A, Maachi R, Chaabane T, Darchen A, Danish M (2022) Aluminum dispersed bamboo activated carbon production for effective removal of Ciprofloxacin hydrochloride antibiotics: Optimization and mechanism study. *J Environ Manage* 301:113765
 19. Guo M, Zhou Z, Yan S, Zhou P, Miao F, Liang S, Wang J, Cui X (2020) Bi₂WO₆-BiOCl heterostructure with enhanced photocatalytic activity for efficient degradation of oxytetracycline. *Sci Rep* 10:18401
 20. Guo Y, Zeng Z, Zhu Y, Huang Z, Cui Y, Yang J (2018) Catalytic oxidation of aqueous organic contaminants by persulfate activated with sulfur-doped hierarchically porous carbon derived from thiophene. *Appl Catal B* 220:635–644
 21. Herrera-Herrera AV, Hernandez-Borges J, Borges-Miquel TM, Rodriguez-Delgado MA (2010) Dispersive liquid-liquid microextraction combined with nonaqueous capillary electrophoresis for the

- determination of fluoroquinolone antibiotics in waters. *Electrophoresis* 31:3457–3465
22. Hu X, Zhao H, Liang Y, Chen F, Li J, Chen R (2021) Broad-spectrum response NCQDs/Bi₂O₂CO₃ heterojunction nanosheets for ciprofloxacin photodegradation: Unraveling the unique roles of NCQDs upon different light irradiation. *Chemosphere* 264:128434
 23. Huang ZH, Ji ZY, Zhao YY, Liu J, Li F, Yuan JS (2020) : Treatment of wastewater containing 2-methoxyphenol by persulfate with thermal and alkali synergistic activation: Kinetics and mechanism. *Chemical Engineering Journal* 380
 24. Ji Y, Dong C, Kong D, Lu J, Zhou Q (2015) Heat-activated persulfate oxidation of atrazine: Implications for remediation of groundwater contaminated by herbicides. *Chem Eng J* 263:45–54
 25. Jia Z, Li T, Zheng Z, Zhang J, Liu J, Li R, Wang Y, Zhang X, Wang Y, Fan C (2020) : The BiOCl/diatomite composites for rapid photocatalytic degradation of ciprofloxacin: Efficiency, toxicity evaluation, mechanisms and pathways. *Chemical Engineering Journal* 380
 26. Jin X, Wu Y, Lin Z, Liang D, Wang F, Zheng X, Liu H, Lv W, Liu G (2022) Plasmonic Ag nanoparticles decorated copper-phenylacetylide polymer for visible-light-driven photocatalytic reduction of Cr(VI) and degradation of PPCPs: Performance, kinetics, and mechanism. *J Hazard Mater* 425:127599
 27. Kumar A, Khan M, Fang L, Lo IMC (2019) Visible-light-driven N-TiO₂@SiO₂@Fe₃O₄ magnetic nanophotocatalysts: Synthesis, characterization, and photocatalytic degradation of PPCPs. *J Hazard Mater* 370:108–116
 28. Li D, Huang J, Li R, Chen P, Chen D, Cai M, Liu H, Feng Y, Lv W, Liu G (2021) Synthesis of a carbon dots modified g-C₃N₄/SnO₂ Z-scheme photocatalyst with superior photocatalytic activity for PPCPs degradation under visible light irradiation. *J Hazard Mater* 401:123257
 29. Li J, Ji Q, Lai B, Yuan D (2017) Degradation of p -nitrophenol by Fe⁰/H₂O₂/persulfate system: Optimization, performance and mechanisms. *J Taiwan Inst Chem Eng* 80:686–694
 30. Li Z, Ma B, Zhang X, Sang Y, Liu H (2020) One-pot synthesis of BiOCl nanosheets with dual functional carbon for ultra-highly efficient photocatalytic degradation of RhB. *Environ Res* 182:109077
 31. Liang H, Yu M, Guo J, Zhan R, Chen J, Li D, Zhang L, Niu J (2021) : A novel vacancy-strengthened Z-scheme g-C₃N₄/Bp/MoS₂ composite for super-efficient visible-light photocatalytic degradation of ciprofloxacin. *Separation and Purification Technology* 272
 32. Liu C, Mao S, Shi M, Wang F, Xia M, Chen Q, Ju X (2021a) Peroxymonosulfate activation through 2D/2D Z-scheme CoAl-LDH/BiOBr photocatalyst under visible light for ciprofloxacin degradation. *J Hazard Mater* 420:126613
 33. Liu C, Mao S, Shi M, Wang F, Xia M, Chen Q, Ju X (2021b) : Peroxymonosulfate activation through 2D/2D Z-scheme CoAl-LDH/BiOBr photocatalyst under visible light for ciprofloxacin degradation. *Journal of Hazardous Materials* 420
 34. Liu S, Gao J, Zhang L, Yang Y, Liu X (2021c) Diethylenetriaminepentaacetic acid-thiourea-modified magnetic chitosan for adsorption of hexavalent chromium from aqueous solutions. *Carbohydr*

35. Liu W, Wang S, Zhao Y, Sun C, Xu H, Zhao J (2021d) : PVP-induced Bi₂S₃/BiOCl photocatalyst with open hollow structures for the removal of ciprofloxacin under visible-light irradiation. *Journal of Alloys and Compounds* 861
36. Llorca M, Farre M, Eljarrat E, Diaz-Cruz S, Rodriguez-Mozaz S, Wunderlin D, Barcelo D (2017) Review of emerging contaminants in aquatic biota from Latin America: 2002–2016. *Environ Toxicol Chem* 36:1716–1727
37. Lominchar MA, Santos A, de Miguel E, Romero A (2018) Remediation of aged diesel contaminated soil by alkaline activated persulfate. *Sci Total Environ* 622–623:41–48
38. Mi Y, Wen L, Wang Z, Cao D, Xu R, Fang Y, Zhou Y, Lei Y (2016) Fe(III) modified BiOCl ultrathin nanosheet towards high-efficient visible-light photocatalyst. *Nano Energy* 30:109–117
39. Miao S, Zha Z, Li Y, Geng X, Yang J, Cui S, Yang J (2019) : Visible-light-driven MIL-53(Fe)/BiOCl composite assisted by persulfate: Photocatalytic performance and mechanism. *Journal of Photochemistry and Photobiology A: Chemistry* 380
40. Paul Chowdhury A, Shambharkar BH (2019) Synthesis and characterization of BiOCl-CoWO₄ nanocomposites with improved photocatalytic activity. *Int J Appl Ceram Technol* 17:1467–1478
41. Peng R, Kang Y, Deng X, Zhang X, Xie F, Wang H, Liu W (2021) : Topotactic transformed face-to-face heterojunction of BiOCl/Bi₂WO₆ for improved tetracycline photodegradation. *Journal of Environmental Chemical Engineering* 9
42. Reichert G, Hilgert S, Fuchs S, Azevedo JCR (2019) Emerging contaminants and antibiotic resistance in the different environmental matrices of Latin America. *Environ Pollut* 255:113140
43. Riaz L, Mahmood T, Kamal A, Shafqat M, Rashid A (2017) Industrial release of fluoroquinolones (FQs) in the waste water bodies with their associated ecological risk in Pakistan. *Environ Toxicol Pharmacol* 52:14–20
44. Sharma K, Dutta V, Sharma S, Raizada P, Hosseini-Bandegharaei A, Thakur P, Singh P (2019) Recent advances in enhanced photocatalytic activity of bismuth oxyhalides for efficient photocatalysis of organic pollutants in water: A review. *J Ind Eng Chem* 78:1–20
45. Sharma VK, Johnson N, Cizmas L, McDonald TJ, Kim H (2016) A review of the influence of treatment strategies on antibiotic resistant bacteria and antibiotic resistance genes. *Chemosphere* 150:702–714
46. Sun J, Hood ZD, Wu S, Wan P, Sun L, Yang S, Chisholm MF (2019a) Reversibly tuning the surface state of Ag via the assistance of photocatalysis in Ag/BiOCl. *Nanotechnology* 30:305601
47. Sun Y, Zhao J, Zhang B-T, Li J, Shi Y, Zhang Y (2019b) Oxidative degradation of chloroxylenol in aqueous solution by thermally activated persulfate: Kinetics, mechanisms and toxicities. *Chem Eng J* 368:553–563
48. Tahmasebi N, Maleki Z, Farahnak P (2019) Enhanced photocatalytic activities of Bi₂WO₆/BiOCl composite synthesized by one-step hydrothermal method with the assistance of HCl. *Mater Sci*

49. Tang J, Zhao B, Lyu H, Li D (2021) : Development of a novel pyrite/biochar composite (BM-FeS₂@BC) by ball milling for aqueous Cr(VI) removal and its mechanisms. *Journal of Hazardous Materials* 413
50. Tian F, Li G, Zhao H, Chen F, Li M, Liu Y, Chen R (2019) Residual Fe enhances the activity of BiOCl hierarchical nanostructure for hydrogen peroxide activation. *J Catal* 370:265–273
51. Walpen N, Joss A, von Gunten U (2021) Application of UV absorbance and electron-donating capacity as surrogates for micropollutant abatement during full-scale ozonation of secondary-treated wastewater. *Water Res* 209:117858
52. Wang Q, Li P, Zhang Z, Jiang C, Zuoqiao K, Liu J, Wang Y (2019) Kinetics and mechanism insights into the photodegradation of tetracycline hydrochloride and ofloxacin mixed antibiotics with the flower-like BiOCl/TiO₂ heterojunction. *J Photochem Photobiol A* 378:114–124
53. Wang Q, Rao P, Li G, Dong L, Zhang X, Shao Y, Gao N, Chu W, Xu B, An N, Deng J (2020) Degradation of imidacloprid by UV-activated persulfate and peroxymonosulfate processes: Kinetics, impact of key factors and degradation pathway. *Ecotoxicol Environ Saf* 187:109779
54. Wang X, Ni Q, Zeng D, Liao G, Wen Y, Shan B, Xie C (2017) BiOCl/TiO₂ heterojunction network with high energy facet exposed for highly efficient photocatalytic degradation of benzene. *Appl Surf Sci* 396:590–598
55. Wang X, Chen Z, Wang Y, Sun W (2021) A review on degradation of perfluorinated compounds based on ultraviolet advanced oxidation. *Environ Pollut* 291:118014
56. Wang Y, Liu C, Zhang Y, Meng W, Yu B, Pu S, Yuan D, Qi F, Xu B, Chu W (2018) Sulfate radical-based photo-Fenton reaction derived by CuBi₂O₄ and its composites with α-Bi₂O₃ under visible light irradiation: Catalyst fabrication, performance and reaction mechanism. *Appl Catal B* 235:264–273
57. Weng C-H, Tao H (2018) Highly efficient persulfate oxidation process activated with Fe⁰ aggregate for decolorization of reactive azo dye Remazol Golden Yellow. *Arab J Chem* 11:1292–1300
58. Wu Y, Ji H, Liu Q, Sun Z, Li P, Ding P, Guo M, Yi X, Xu W, Wang CC, Gao S, Wang Q, Liu W, Chen S (2022) Visible light photocatalytic degradation of sulfanilamide enhanced by Mo doping of BiOBr nanoflowers. *J Hazard Mater* 424:127563
59. Xiang Q, Yu J, Wang W, Jaroniec M (2011) Nitrogen self-doped nanosized TiO₂ sheets with exposed {001} facets for enhanced visible-light photocatalytic activity. *Chem Commun (Camb)* 47:6906–6908
60. Yan C, Yang Y, Zhou J, Liu M, Nie M, Shi H, Gu L (2013) Antibiotics in the surface water of the Yangtze Estuary: occurrence, distribution and risk assessment. *Environ Pollut* 175:22–29
61. Yang Z, Li X, Huang Y, Chen Y, Wang A, Wang Y, Li C, Hu Z, Yan K (2021) : Facile synthesis of cobalt-iron layered double hydroxides nanosheets for direct activation of peroxymonosulfate (PMS) during degradation of fluoroquinolones antibiotics. *Journal of Cleaner Production* 310
62. Yao J, Wen J, Li H, Yang Y (2022) Surface functional groups determine adsorption of pharmaceuticals and personal care products on polypropylene microplastics. *J Hazard Mater*

63. Yu F, Sun Y, Yang M, Ma J (2019a) Adsorption mechanism and effect of moisture contents on ciprofloxacin removal by three-dimensional porous graphene hydrogel. *J Hazard Mater* 374:195–202
64. Yu X, Zhang J, Zhang J, Niu J, Zhao J, Wei Y, Yao B (2019b) Photocatalytic degradation of ciprofloxacin using Zn-doped Cu₂O particles: Analysis of degradation pathways and intermediates. *Chem Eng J* 374:316–327
65. Zhang F, Wang X, Liu H, Liu C, Wan Y, Long Y, Cai Z (2019a) :Recent Advances and Applications of Semiconductor Photocatalytic Technology. *Applied Sciences* 9
66. Zhang H, Wu W, Li Y, Wang Y, Zhang C, Zhang W, Wang L, Niu L (2019b) Enhanced photocatalytic degradation of ciprofloxacin using novel C-dot@Nitrogen deficient g-C₃N₄: Synergistic effect of nitrogen defects and C-dots. *Appl Surf Sci* 465:450–458
67. Zhang L, Gao Y, Yue Q, Zhang P, Wang Y, Gao B (2020a) Preparation and application of novel blast furnace dust based catalytic-ceramic-filler in electrolysis assisted catalytic micro-electrolysis system for ciprofloxacin wastewater treatment. *J Hazard Mater* 383:121215
68. Zhang XX, Dong LL, Cai K, Li RP (2013) A Routine Method for Simultaneous Determination of Three Classes of Antibiotics in Aquaculture Water by SPE-RPLC-UV. *Adv Mater Res* 726–731:1253–1259
69. Zhang Y, Shao Q, Jiang H, Liu L, Wu M, Lin J, Zhang J, Wu S, Dong M, Guo Z (2020b) One-step co-precipitation synthesis of novel BiOCl/CeO₂ composites with enhanced photodegradation of rhodamine B. *Inorg Chem Front* 7:1345–1361
70. Zhao C, Li Y, Chu H, Pan X, Ling L, Wang P, Fu H, Wang C-C, Wang Z (2021a) : Construction of direct Z-scheme Bi₅O₇I/UiO-66-NH₂ heterojunction photocatalysts for enhanced degradation of ciprofloxacin: Mechanism insight, pathway analysis and toxicity evaluation. *Journal of Hazardous Materials* 419
71. Zhao C, Pan X, Wang Z, Wang C-C (2021b) : 1 + 1 > 2: A critical review of MOF/bismuth-based semiconductor composites for boosted photocatalysis. *Chemical Engineering Journal* 417
72. Zhao R, Wang Y, An Y, Yang L, Sun Q, Ma J, Zheng H (2022) Chitin-biocalcium as a novel superior composite for ciprofloxacin removal: Synergism of adsorption and flocculation. *J Hazard Mater* 423:126917
73. Zhong X, Zhang K-X, Wu D, Ye X-Y, Huang W, Zhou B-X (2020) : Enhanced photocatalytic degradation of levofloxacin by Fe-doped BiOCl nanosheets under LED light irradiation. *Chemical Engineering Journal* 383
74. Zhou JL, Kang Y (2013) Matrix effect in high-performance liquid chromatography-tandem mass spectrometry analysis of antibiotics in environmental water samples. *J Sep Sci* 36:564–571
75. Zhou Y-n, Li R, Tao L, Li R, Wang X, Ning P (2020) : Solvents mediated-synthesis of 3D-BiOX (X = Cl, Br, I) microspheres for photocatalytic removal of gaseous Hg⁰ from the zinc smelting flue gas. *Fuel* 268

76. Zhu H, Yang B, Yang J, Yuan Y, Zhang J (2021) Persulfate-enhanced degradation of ciprofloxacin with SiC/g-C₃N₄ photocatalyst under visible light irradiation. *Chemosphere* 276:130217
77. Zhu J, Shen Y, Yu X, Guo J, Zhu Y, Zhang Y (2019) A facile two-step method to synthesize immobilized CdS/BiOCl film photocatalysts with enhanced photocatalytic activities. *J Alloys Compd* 771:309–316
78. Zhuang J, Rong N, Wang X, Chen C, Xu Z (2022) : Adsorption of small size microplastics based on cellulose nanofiber aerogel modified by quaternary ammonium salt in water. *Separation and Purification Technology* 293
79. Zou S, Xu W, Zhang R, Tang J, Chen Y, Zhang G (2011) Occurrence and distribution of antibiotics in coastal water of the Bohai Bay, China: impacts of river discharge and aquaculture activities. *Environ Pollut* 159:2913–2920

Unsectioned Paragraphs

Tel: +86-13844908048, Fax: +86-431-84566150.

Supplementary Files

This is a list of supplementary files associated with this preprint. Click to download.

- [SupplementaryMaterial.docx](#)